PERGAMON

International Journal of Solids and Structures 38 (2001) 5335–5353

INTERNATIONAL JOURNAL OF SOLIDS and STRUCTURES

www.elsevier.com/locate/ijsolstr

Expert drawbead models for finite element analysis of sheet metal forming processes

Y.T. Keum *, J.H. Kim, B.Y. Ghoo

Division of Mechanical Engineering, Hanyang University, 17 Haengdang-Tong, Sungdong-Ku, Seoul 133-791 South Korea

Received 15 October 1999

Abstract

The expert drawbead model which computes the drawing characteristics of the drawbead used in a finite element analysis of sheet metal forming processes is developed. The mathematical models of the basic drawbeads such as the circular drawbead, stepped drawbead, and squared drawbead, whose dimensions and processes are various, are first derived using the bending theory, belt-pulley equation, and Coulomb friction law. Next, the experiments for finding the drawing characteristics of the drawbead are performed. Based on the mathematical model, the expert model of the basic drawbead is then developed employing a linear multiple regression method by which the difference in drawing characteristics between the drawing test and the mathematical model is minimized. For the expert models of combined drawbeads such as the double circular drawbead, double stepped drawbead, circular-and-stepped drawbead, etc., those of the basic drawbeads are summed. Finally, to verify the expert models developed, the drawbead restraining force and bead-exit pre-strain calculated by the expert models of the double circular drawbead and circular-and-stepped drawbead are compared with those obtained from the experiments. The predictions by expert models agree well with the measurements by the experiments.

Keywords: Expert drawbead model; Sheet forming analysis; Drawbead restraining force; Pre-strain; Linear multiple regression method

1. Introduction

The considerable tryouts by trials and errors in stamping die design are inevitable because the stamping variables such as tool geometry, friction, drawbead, binder/blank holding force (BHF), etc., are various. To reduce the tryouts which consume a great deal of time, it is very important for a die designer to make a precise decision about the fitness of the drawbead used to control the flow of the sheet into the die cavity in the early design stages. If the design of the drawbeads is not suitable, it makes the sheet stretch or draw excessively because the restraining force incorrectly acts on the sheet. In general, improper design of the drawbeads is unavoidable because the drawbeads are usually not only designed intuitively by a designer's know-how but also manufactured empirically by hand grinding and welding without a theoretical background.

* Corresponding author. Tel.: +82-2-2290-0436; fax: +82-2-2298-6194.
E-mail address: ytkeum@email.hanyang.ac.kr (Y.T. Keum).

0020-7683/01/$ - see front matter
PII: S0020-7683(00)00342-5

The drawbead design based on mechanics has been a long-cherished desire to many die designers and engineers in sheet metal forming. When drawbead design is carried out through systematic analyses, the tedious tryouts can be reduced tremendously. Furthermore, as the restraining force and bead-exit pre-strain are usually boundary conditions in numerical analyses of sheet metal forming processes, an accurate description of drawing characteristics of the drawbead has also been an earnest wish to many numerical analysts.

For the systematic establishment of theory of drawbead design, it is necessary to make a database on the technical know-how, experimental measurements, and numerical analyses of the drawbeads. The pre-estimate theory for the drawing characteristics such as restraining force, bead-exit pre-strain, etc. is especially needed.

During the last 20 years, some drawbead models have been proposed from quite simple ones to very sophisticated ones. In this research, they are historically reviewed. In the 1970s and 1980s, Nine (1978, 1982) investigated stamping variables affecting a drawbead restraining force (DBRF) and proposed a DBRF and bead-exit pre-strain at the upper and lower skins of the sheet when a circular drawbead is employed in a binder-holding process. Also, Wang (1982) formulated a mathematical model of circular drawbeads and evaluated the DBRF considering bending, sliding, and unbending. Using the virtual work principle, Levy (1983) predicted a DBRF introducing the anisotropic and strain rate parameters of a sheet. Weinmann and Sanchez (1988) analyzed the DBRF of circular drawbeads which they assumed as rollers. Stoughton (1988) presented a mathematical model of drawbeads in which the work required to pull a sheet through the drawbead is equated to the work required to bend and straighten the sheet and to overcome the frictional forces in sliding over the bend radii. Ujohara et al. (1988) calculated drawbead restraining forces and strains using the belt-pulley theory.

In 1990s, Wang and Shah (1991) evaluated the effects of drawbead dimensions and friction coefficients. Kojima (1993) presented that drawbead effects for controlling draw-ins of a sheet are simplified to the restraining force working at a drawbead position. Demeri (1993) assessed the influence of material properties, drawbead penetration, and lubricating condition on the sheet flow. Sunaga et al. (1996) proposed an efficient method to determine the DBRF, which provided for a finite element code to simulate the forming process of automotive panels. It was reported that a 2-D finite element simulation was able to provide an accurate enough DBRF, which was calculated only from the contact angle between the sheet and drawbead, for arbitrary drawbead dimensions without real an experiment. Carleer et al. (1996) implemented the effects of the restraining force and bead-exit pre-strain in an equivalent drawbead by using the drawbead stiffness. The restraining force reaches its steady state value when a part of the sheet has been pulled entirely through the drawbead (Cao and Boyce, 1993). You et al. (1998) proposed a numerical model for the calculation of DBRF. The kinematics hardening rule and the Bauschinger effect are considered in their model. Meinders et al. (1998) applied an equivalent drawbead model based on a penalty constraint method for the simulations of deep drawing processes. For the equivalent drawbead model, the DBRF, plastic thickness strain, and lift force are obtained from a 2-D finite element drawbead model.

Although many researchers have proposed drawbead models positioned in the direction normal to the sheet movement, drawbead models with an arbitrary angle have hardly been introduced.

In this research, expert drawbead models which provide the drawing characteristics of the drawbead used in the finite element analysis of sheet metal forming processes are proposed. The mathematical models of the drawbeads are at first derived using the bending theory, belt-pulley equation, and the Coulomb friction law. To find the drawing characteristics of the drawbeads, drawing tests are then performed. To minimize the difference in drawing characteristics between a drawing test and a mathematical model, a linear multiple regression method is next employed. In order to verify the expert drawbead models developed, finally, the drawing characteristics predicted by the expert models of combined drawbeads are compared with those measured in the experiments.

2. Mathematical models

The mathematical models of the basic drawbeads, namely, circular drawbead, stepped drawbead, and squared drawbead are derived to calculate the DBRF and drawbead-exit pre-strain, which can be used as boundary conditions in the FEM simulation of forming processes.

The DBRF required to pass over the drawbead with an arbitrary angle can be divided into the components of the normal and tangential directions to the drawbead. The normal component of the DBRF can be obtained by investigating the force mechanism when the sheet passes the surface with curvatures, and the tangential component may be calculated by considering that when it slips along the drawbead.

When the sheet is drawn out through the drawbead, the bending and tension bring out strains called a drawbead-exit pre-strain. The strains by the tensions in the normal and tangential directions to the drawbead are assumed to be obtained by the normal and tangential DBRFs, respectively.

2.1. Circular drawbead

Fig. 1 shows the DBRF and its normal and tangential components in a single circular drawbead positioned with an arbitrary angle to a material moving direction.

From the sectional geometry of a circular drawbead and a formed sheet shown in Fig. 2, the normal drawbead restraining force, $DBRF_n$, is computed from the elastic force, frictional force, upper pressure, tension, and bending/unbending force (Stoughton, 1988).

The elastic deformation is due to the initial elastic displacement of the sheet when the drawbead closes and it can be determined from the maximum displacement of a fixed beam. The elastic force, F_e, and the displacement, δ, are respectively derived as follows (Stoughton, 1988):

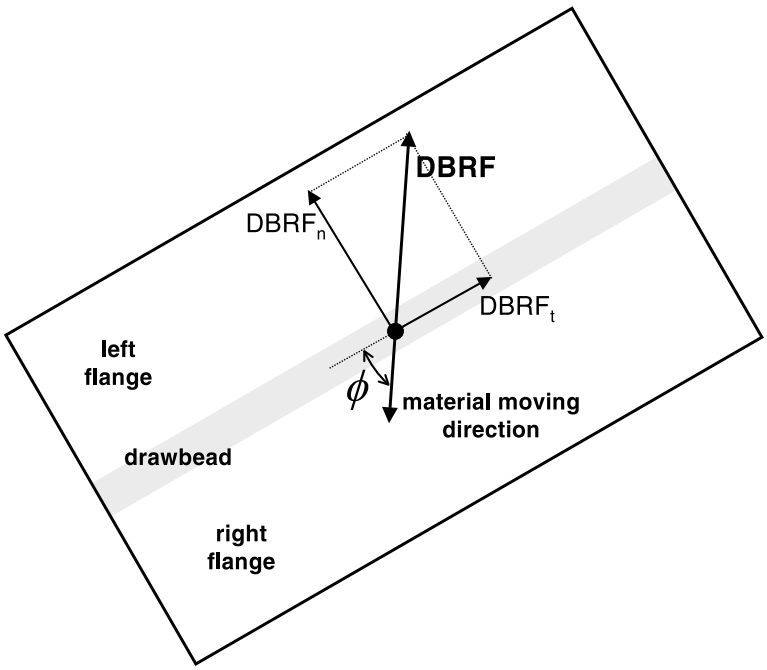

Fig. 1. DBRF in the drawbead located with an arbitrary angle (ϕ) to the material moving direction.

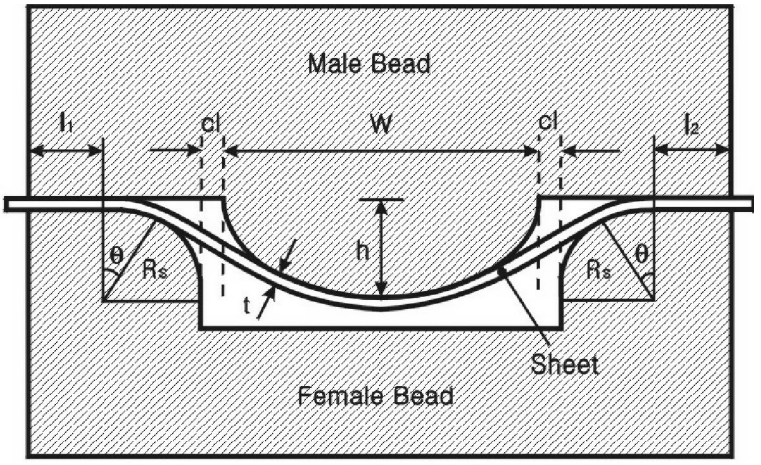

Fig. 2. Section view of a single circular drawbead and a formed sheet.

$$F_e = \frac{16Ew\delta t^3}{(2R_s + W + 2\mathrm{cl})^3} \tag{1}$$

$$\delta = \min\left(h, 2(2R + t)\frac{RY_p}{tE}\right) \tag{2}$$

where E, Y_p, w, and t are the elastic modulus, yield stress, width, and thickness of the sheet, respectively. R_s, W, h, R, and cl are the radius of female bead, the width of male bead, the height of male bead, the radius of male bead, and the clearance between the female bead and male bead, respectively (see Fig. 2). A detailed description of the sheet formed by a circular drawbead is shown in Fig. 3. To keep the state of the male and female beads fully closed, the BHF exerted is usually greater than the upper pressure.

The discrepancy between the BHF and the upper pressure contributes to the frictional forces on both flanges. If l_1 and l_2 are left and right flange lengths (see Fig. 2), the frictional forces in the left and right flanges, F_{c1} and F_{c2}, can be respectively derived as follows:

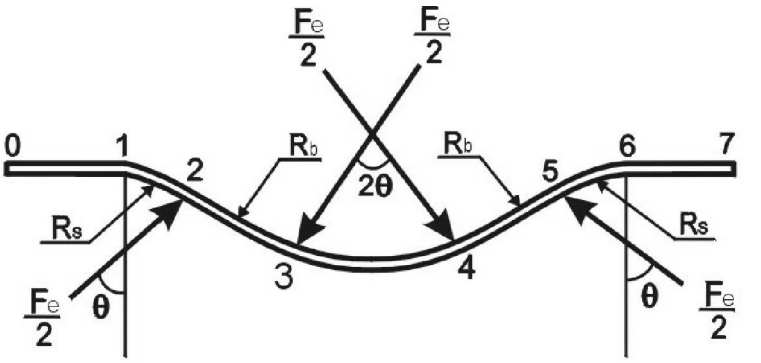

Fig. 3. Detail description of the sheet formed by a single circular drawbead.

$$F_{c1} = 2\mu\left[\frac{l_1}{l_1 + l_2}\mathrm{BHF}\right] - 2\mu\left[\frac{l_1}{l_1 + l_2 + W + 2R_s}F_R\right] \tag{3}$$

$$F_{c2} = 2\mu\left[\frac{l_2}{l_1 + l_2}\mathrm{BHF}\right] - 2\mu\left[\frac{l_2}{l_1 + l_2 + W + 2R_s}F_R\right] \tag{4}$$

where μ, BHF, and F_R are the friction coefficient, blank holding force, and upper pressure of the circular drawbead, respectively. The force at point 1, F_1, is given to the bending force when the thickness is equal to the initial one and the strain in the drawing direction is zero. In the region from point 1 to point 2, the force is calculated by multiplying $e^{\mu\theta}$ to the force before the bending. The successive unbending force acts on the material at point 2. The frictional force, $\mu(F_e/2)$, also acts on the sheet. At point 3, the bending force, F_3, as well as the frictional force, $\mu(F_e/2)$, acts on the sheet by elastic force. In the region from point 3 to point 4, the force after the sliding is obtained by multiplying $e^{\mu\theta}$ to the force before the bending. Because the unbending force at point 4, F_4, the frictional force, μF_e, from point 4 to point 5, the bending force, F_5, at point 5, the frictional force, μF_e, from point 5 to point 6, the unbending force, F_6, at point 6, and the frictional force existing in the right flange, F_{c2}, act on the sheet metal in due sequence, the normal component of the drawbead restraining force, $\mathrm{DBRF_n}$, is,

$$\mathrm{DBRF_n} = \lfloor\{(F_{c1} + F_1)e^{\mu\theta} + F_2 + \mu F_e + F_3\}e^{2\mu\theta} + F_4 + \mu F_e + F_5\rfloor e^{\mu\theta} + F_6 + F_{c2} \tag{5}$$

When the sheet passes over the circular drawbead, a free body diagram of the upper male bead in the normal direction is depicted as in Fig. 4. The upper pressure of the circular drawbead is the sum of the

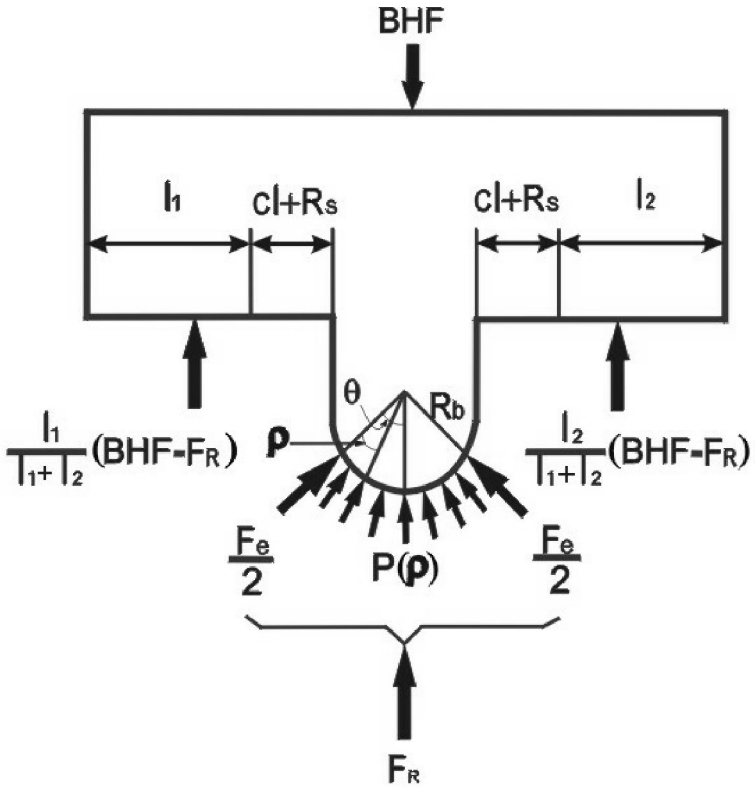

Fig. 4. Free body diagram of a male bead in a single circular drawbead.

vertical components of elastic forces and frictional forces. The vertical components of the total forces, B, generated by the pressure distribution, $P(\rho)$, acting on the drawbead surface, can be computed as follows:

$$B = \int_0^{2\theta} F_0 e^{\mu\theta} \cos(\theta - \rho)\, d\rho = F_0 G(\mu, \theta) \tag{6}$$

where ρ is the loading angle of $P(\rho)$ as defined in Fig. 4, F_0 is the force when $\rho = 0$, and θ is the contact angle between the sheet and the bead, respectively. Therefore, using Eqs. (1) and (6), the upper pressure of the circular drawbead, F_R, is written as follows:

$$F_R = F_0 G(\mu, \theta) + F_e \cos\theta \tag{7}$$

In Eq. (7), F_0 is expressed as follows:

$$F_0 = \lfloor (F_{c1} + F_1) e^{\mu\theta} + \mu F_e + F_2 + F_3 \rfloor \tag{8}$$

By virtue of Eqs. (3), (6) and (8), the upper pressure, F_R, is derived from Eq. (7) as follows:

$$F_R = \frac{F_e \cos\theta + (F_1 e^{\mu\theta} + 2\mu \mathrm{BHF} e^{\mu\theta} l_1/(l_1 + l_2) + \mu F_e + F_2 + F_3) G(\mu, \theta)}{1 + 2\mu G(\mu, \theta) e^{\mu\theta} l_1/(l_1 + l_2)} \tag{9}$$

When the sheet passes over the drawbead, it is situated on the action of bending and unbending. The bending or unbending force can be derived by equating the work required to pull the sheet through the drawbead to it to bend and straighten the sheet (Stoughton, 1988). Assuming that the compression energy equals the tension energy when the sheet is bended, the bending force is derived as follows:

$$F_i = w \int_{t_n}^{t_i} dy \int_{\varepsilon_i}^{\varepsilon(y)} \sigma\, d\varepsilon + w \int_{t_n}^{2t_n} dy \int_{\varepsilon_i}^{\varepsilon(y)} \sigma\, d\varepsilon \tag{10}$$

where w, t_i, t_n, and y are sheet width, sheet thickness before bending, distance from the bottom to the neutral surface of the sheet, and distance from the bottom to any point of the sheet, respectively. In Eq. (10), the strain, $\varepsilon(y)$, and the strain rate at the point y, $\dot{\varepsilon}(y)$, which is used in the plastic constitutive equation are defined as follows:

$$\varepsilon(y) = \varepsilon_i + \frac{1 + r}{\sqrt{1 + 2r}} \ln\left(\frac{R_{\mathrm{eff}} + y}{R_{\mathrm{eff}} + t_n}\right) \tag{11}$$

$$\dot{\varepsilon}(y) = \varepsilon(y) \frac{v}{t_i} \left(\frac{R_{\mathrm{eff}} + y}{R_{\mathrm{eff}} + t_n}\right) \tag{12}$$

where ε_i, r, R_{eff}, v are pre-strain before bending, plastic anisotropy parameter, effective radius of curvature, and drawing velocity, respectively. Ignoring the effect of the strain rate on the bending and using Eqs. (10)–(12), the bending force, F_i, is derived as follows:

$$F_i = \frac{wK(R_{\mathrm{eff}} + t_n)}{n + 1} f\left(\varepsilon_m \frac{v}{t_i} \frac{R_{\mathrm{eff}} + t_i}{R_{\mathrm{eff}} + t_n}, \dot{\varepsilon}_0, m\right) \left[\int_0^{\frac{\sqrt{1+2r}}{1+r}\varepsilon_m} \left\{ \left[\varepsilon_i + \frac{1 + r}{\sqrt{1 + 2r}} \zeta\right]^{1+n} - \varepsilon_i^{1+n} \right\} e^{\zeta} d\zeta + \int_0^{\ln \frac{R_{\mathrm{eff}} + 2t_n}{R_{\mathrm{eff}} + t_n}} \left\{ \left[\varepsilon_i + \frac{1 + r}{\sqrt{1 + 2r}} \zeta\right]^{1+n} - \varepsilon_i^{1+n} \right\} e^{\zeta} d\zeta \right] \tag{13}$$

where K, m, and n are the strength coefficient, strain rate sensitivity exponent, and strain hardening exponent, respectively. In Eq. (13), ζ and ε_m are the intermediate variable and strain at the outer surface, respectively, which are defined as follows:

$$\zeta = \ln \frac{R_{\text{eff}} + y}{R_{\text{eff}} + t_{\text{n}}}. \tag{14}$$

$$\varepsilon_m = \frac{1+r}{\sqrt{1+2r}} \ln \left(\frac{1 + t_i/R_{\text{eff}}}{1 + t_{\text{n}}/R_{\text{eff}}} \right) \tag{15}$$

When the sheet passes over the drawbead which is located with an arbitrary angle, ϕ, to the material moving direction, the tangential component of drawbead restraining force, DBRF_{t}, is derived as follows just considering the frictional force:

$$\text{DBRF}_{\text{t}} = \left\{ F_{\text{c1}} + F_{\text{c2}} + \mu \left(F_{\text{e}} + F_R \frac{W}{l_1 + l_2 + W + 2R_{\text{s}}} \right) + \mu F_{\text{e}} \right\} \cos(\phi) \tag{16}$$

When the sheet is drawn out, the effective stress, $\overline{\sigma}$, and the effective strain, $\overline{\varepsilon}$, may be respectively represented as follows employing Hill's old theory:

$$\overline{\sigma} = \left[\frac{(1+2r)(\sigma_{\text{n}} - \sigma_{\text{t}})^2 + (\sigma_{\text{n}} + \sigma_{\text{t}})^2}{2(1+r)} \right]^{1/2} \tag{17}$$

$$\overline{\varepsilon} = \left[\frac{\overline{\sigma}}{K} \right]^{1/n} \tag{18}$$

where σ_{n} and σ_{t} are respectively the stresses caused by the normal and tangential DBRFs.

By virtue of Eqs. (17) and (18), and the associated flow rule, the strain in the normal direction to the drawbead, ε_{n} is derived as follows ignoring strain-rate effects:

$$\varepsilon_{\text{n}} = \varepsilon_{\text{b}} + \{(1+r)\sigma_{\text{n}} - r\sigma_{\text{t}}\} \left[\frac{\overline{\sigma}^{(1-n)/n}}{K^{1/n}(1+r)} \right] \tag{19}$$

where ε_{b} is the strain by the bending and unbending.

When the sheet slips along the drawbead, since no change in the curvature occurs, the effect of the bending and unbending on the tangential strain can be ignorable so that the strain in the tangential direction to the drawbead, ε_{t} is showed as follows:

$$\varepsilon_{\text{t}} = \{ -r\sigma_{\text{n}} + (1+r)\sigma_{\text{t}} \} \left[\frac{\overline{\sigma}^{(1-n)/n}}{K^{1/n}(1+r)} \right] \tag{20}$$

2.2. Stepped drawbead

From the sectional view of a stepped drawbead and a formed sheet shown in Fig. 5, the normal drawbead restraining force, DBRF_{n}, is computed from the elastic force, frictional force, upper pressure, tension, and bending/unbending force. The ways of the equation derivation of the stepped drawbead are similar to those of the circular drawbead. The elastic force, F_{e}, is expressed as follows by the fixed beam theory:

$$F_{\text{e}} = \frac{16Ew\delta t^3}{(4R + 2\text{cl})^3} \tag{21}$$

where R is the radius of the upper bead and δ is defined as in Eq. (2)

The sheet formed by a stepped drawbead is shown in Fig. 6. It is assumed that the frictional forces in the contact area are derivable from the discrepancy between BHF and upper pressure. If l_1 and l_2 are left and

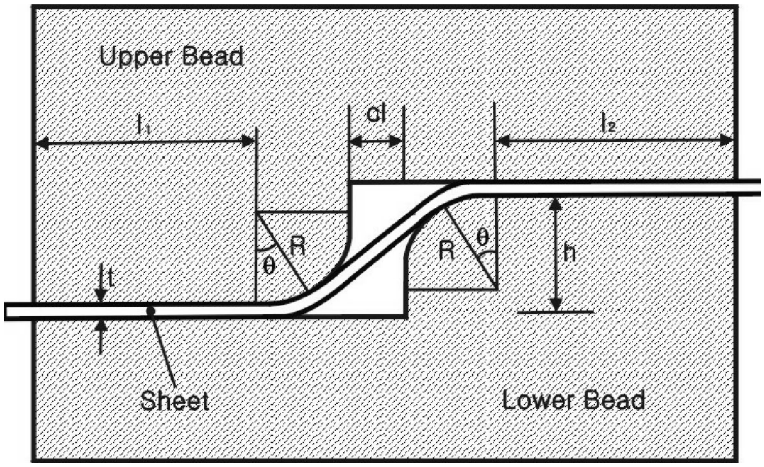

Fig. 5. Sectional view of a stepped drawbead and a formed sheet.

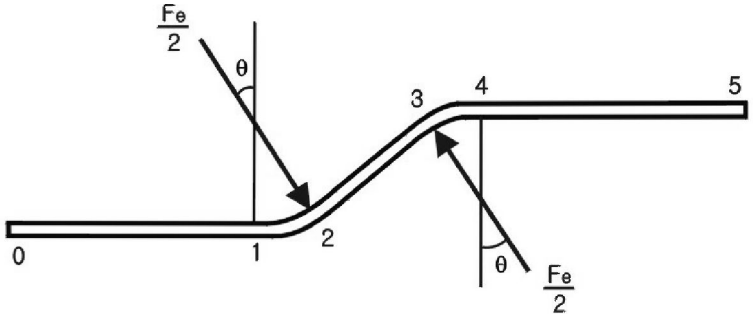

Fig. 6. Detail description of the sheet formed by a stepped drawbead.

right flange lengths (see Fig. 5), the frictional forces in the left and right flanges, F_{c1} and F_{c2}, can be respectively expressed as follows:

$$F_{c1} = 2\mu(\mathrm{BHF} - F_R)\left[\frac{l_1}{l_1 + l_2 + 2R}\right] \tag{22}$$

$$F_{c2} = 2\mu(\mathrm{BHF} - F_R)\left[\frac{l_2}{l_1 + l_2 + 2R}\right] \tag{23}$$

Following the same way as in the circular drawbead, the normal component of the drawbead restraining force of the stepped drawbead, $\mathrm{DBRF_n}$, can be obtained as follows:

$$\mathrm{DBRF_n} = \left\lfloor (F_{c1} + F_1)e^{\mu\theta} + F_2 + \mu F_e + F_3 \right\rfloor e^{\mu\theta} + F_4 + F_{c2} \tag{24}$$

The free body diagram of the upper bead in a stepped drawbead is seen in Fig. 7. The upper pressure, F_R, is written as follows:

$$F_R = B + (F_e/2)\cos\theta \tag{25}$$

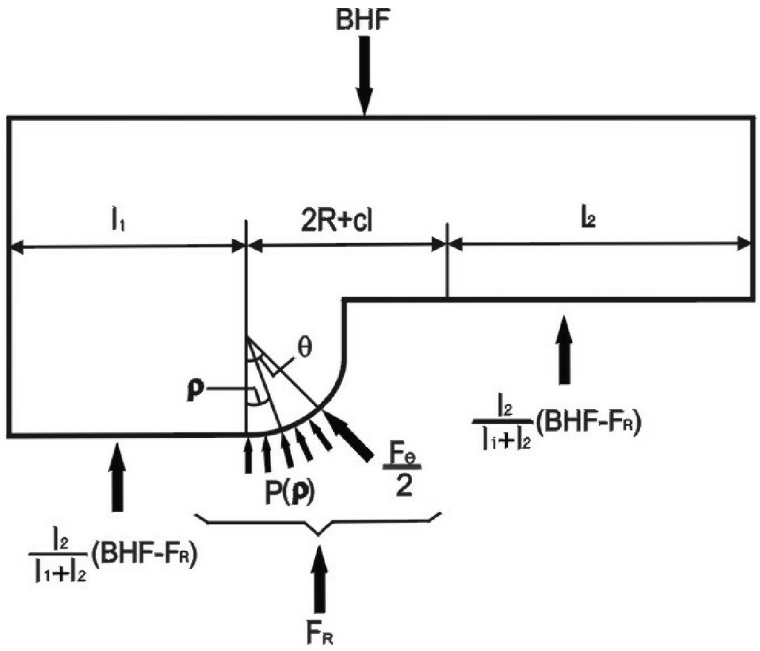

Fig. 7. Free body diagram of a male bead in a stepped drawbead.

where B is the vertical force by the pressure defined as follows:

$$B = \int_0^{\theta} F_0 e^{\mu\rho} \cos\rho \, d\rho = F_0 H(\mu, \theta) \tag{26}$$

where $F_0 = F_{c1} + F_1$. As in the circular drawbead, the form of the upper pressure, F_R, can be given as follows:

$$F_R = \frac{F_e/2 \cos\theta + \lfloor F_1 + 2\mu \mathrm{BHF} l_1/(l_1 + l_2)\rfloor H(\mu, \theta)}{1 + 2\mu H(\mu, \theta) l_1/(l_1 + l_2)} \tag{27}$$

When the sheet passes over the stepped drawbead which is located with an arbitrary angle, ϕ, in the material moving direction, the tangential component of the drawbead restraining force, $\mathrm{DBRF_t}$, is derived as follows:

$$\mathrm{DBRF_t} = \{F_{c1} + F_{c2} + \mu F_e\} \cos(\phi) \tag{28}$$

Ignoring strain-rate effects, in addition, the strains in the normal and tangential directions to the drawbead may be calculated by Eqs. (19) and (20), respectively, as in the circular drawbead.

2.3. Squared drawbead

In general, the stamping die engineers use a squared drawbead when the sheet is not drawn into the die cavity and the sheet is fixed along the boundary of the die surface. So, in this research, the sheet clamped by the squared drawbead is assumed to have a very big DBRF and no bead-exit pre-strain.

3. Experiments

In order to obtain the actual behavior of the drawing characteristics of the drawbeads, the friction testing apparatus originally designed by Nine (1978) and modified by Kim and Kim (1991) is employed. For the friction coefficients associated with different lubricants, the drawing tests are independently performed with a fixed drawbead and a roller drawbead. For the DBRFs and bead-exit pre-strains associated with various drawbeads, the drawing tests are also carried out with the circular drawbeads and the stepped drawbeads, which are located 60°, 75°, and 90° in the material moving direction.

The friction coefficient can be obtained from the Coulomb friction law, which is namely the relationship between normal force and frictional force. In drawing tests, the normal force is the BHF. The frictional force is the difference between the DBRFs obtained in the fixed drawbead and roller drawbead drawing tests. Then, the friction coefficient (μ), which is the ratio of the frictional force to the normal force, may be expressed as follows (Nine, 1978, 1982):

$$\mu = \frac{F_f}{N} = \frac{D_{f+d} - D_d}{\pi C_{f+d}} \tag{29}$$

where F_f and N are respectively frictional force and normal force. In Eq. (29), D_{f+d} and C_{f+d} are the DBRF and BHF measured in the fixed drawbead drawing test, respectively, and D_d is the DBRF observed in the roller drawbead drawing test. The friction coefficients for various sheets and lubricants obtained from Eq. (29) and experiments are listed in Table 1.

To find the DBRF and bead-exit pre-strain, drawing tests in which the fixed drawbead die set in the friction testing apparatus is replaced by a manufactured drawbead die set are performed. Dimensions of the drawbead die set manufactured for drawbead drawing tests are shown in Table 2. The width and length of the sheet specimen are 45 and 300 mm, respectively. While the grip clamping an edge of the specimen is pulled out, the drawing force and displacement are measured. The drawing force at a steady state is supposed to be a DBRF. As an example of experimental measurements, the DBRF and bead-exit pre-strain of a single circular drawbead associated with BHFs, lubricants, and dimensions are shown in Table 3.

Table 1
Friction coefficients for various sheets and lubricants

Sheet	Thickness (mm)	Lubricant	Friction coefficient
SPC1	0.6	BWD-610	0.13
		P-340N	0.19
		DRY	0.17
	0.8	P-340N	0.18
		DRY	0.16
SPC3	0.8	P-340N	0.19
		DRY	0.16
SKY-AL TG25	1.0	P-340N	0.20
		DRY	Failure
SPCC	0.6	P-340N	0.153
		DRY	0.140
	0.8	P-340N	0.159
		DRY	0.146

Table 2
Dimensions of drawbead die set for drawbead drawing tests

Drawbead	Radius of shoulder (mm)		Height (mm)		Drawbead angle (deg)
Circular drawbead	3.8		6		90
			4.5		75
	4.5		3		60
			2		60
Stepped drawbead	3		6		90
			6		75
	4		6		75
			6		60
Double circular drawbead	3.8		6		90
			4.5		90
	4.5		3		90
			2		90
Circular-and-stepped drawbead	Circular drawbead		Stepped drawbead		
	Radius of shoulder (mm)	Height (mm)	Radius (mm)	Height (mm)	
	4.5	3	3	6	90
		6	4	6	90

Table 3
DBRF and bead-exit pre-strain of a circular drawbead for various forming conditions and die dimensions (material: SPCC, bead height: 3 mm, bead radius: 3.8 mm)

BHF (N/mm)	Sheet thickness (mm)	Lubricant	Drawbead angle, ϕ (deg)	DBRF (N/mm)	Pre-strain (%)
110	0.6	DRY	90	60.94	5.08
			75	61.72	3.78
			60	58.61	3.78
	0.8	DRY	90	69.74	6.12
			75	72.37	3.82
			60	67.32	4.47
165	0.6	P-340N	90	80.38	7.72
			75	84.49	5.08
			60	78.14	2.93
		DRY	90	79.21	6.84
			75	79.77	4.65
			60	80.91	4.65
	0.8	P-340N	90	90.55	8.13
			75	97.29	6.78
			60	89.83	5.78
		DRY	90	86.46	7.79
			75	91.91	6.45
			60	88.39	6.12

4. Expert models

The mathematical models described in Section 2 usually have inevitable errors because of the assumption on the geometric modeling, material behavior, and forming processes. To minimize the errors between prediction by mathematical models and measurement by experiments, a linear multiple regression method

is employed, in which the forming process variables and drawbead geometries are used as regression variables to find the most sensitive variable to the errors. After modifying the most sensitive variable by the linear multiple regression method, the drawing characteristics in the mathematical model are obtained using the modified variable to predict more precisely.

Since the mathematical model cannot only provide precise predictions of drawing characteristics using the modified variable but also handle any drawbead geometries, material properties, and process variables, the mathematical model correcting the predictions by the linear multiple regression method is called an expert model in this study.

4.1. Circular drawbead

In order to investigate the effects of drawbead geometries and process variables on the difference between mathematical prediction and experimental measurement, a linear multiple regression method is employed. Since the difference in the DBRF between prediction and measurement is mainly caused by the friction coefficient, the correction factor, a, is introduced in the modified friction coefficient used in the expert model as follows:

$$\mu' = a\mu \tag{30}$$

where a is obtained by substituting Eq. (30) into Eqs. (5) and (16) and by comparing the theoretical predictions with the experimental measurements employing the multiple regression method. If the correction factor, a, is a function of process variables and drawbead dimensions, it is expressed as follows:

$$a = \alpha + \beta\mu + \gamma h + \zeta R_s + \eta t + \kappa \mathrm{BHF} + \psi\phi \tag{31}$$

where R_s, t, and BHF are radius of female bead, thickness of the sheet, and blank holding force, respectively. In Eq. (31), α, β, γ, ζ, η, κ, and ψ are the constants determined by the experimental measurements. For the single circular drawbead, these values are 1.472, −1.951, −0.007, 0.012, −0.004, 0.096, and −0.001, respectively.

4.2. Stepped drawbead

In a similar manner as in the circular drawbead, the friction coefficient, μ, is corrected as follows:

$$\mu' = b\mu \tag{32}$$

where the correction factor, b, can be obtained by the multiple regression method as follows:

$$b = \alpha + \beta\mu + \zeta R + \eta t + \kappa \mathrm{BHF} + \psi\phi \tag{33}$$

where R is the radius of drawbead shoulder. In Eq. (33), α, β, ζ, η, κ, and ψ are the constants determined by the experimental measurements. In this study, these values are found to be 0.959, −1.136, −0.243, 0.079, −0.0002, and −0.0001, respectively.

4.3. Combined drawbead

The DBRF of the combined drawbead such as the double circular drawbead, circular-and-stepped drawbead, double stepped drawbead, etc., is assumed to be expressed as the sum of those of the basic drawbeads. That is, the normal drawbead restraining force, $\mathrm{DBRF}_{\mathrm{Cn}}$, and the tangential drawbead restraining force, $\mathrm{DBRF}_{\mathrm{Ct}}$, of the combined drawbead C, which consists of basic drawbead A and drawbead B, can be given as follows:

$$\mathrm{DBRF}_{\mathrm{Cn}} = \mathrm{DBRF}_{\mathrm{An}} + \mathrm{DBRF}_{\mathrm{Bn}} \tag{34}$$

$$\mathrm{DBRF}_{\mathrm{Ct}} = \mathrm{DBRF}_{\mathrm{At}} + \mathrm{DBRF}_{\mathrm{Bt}} \tag{35}$$

where $\mathrm{DBRF}_{\mathrm{An}}$, $\mathrm{DBRF}_{\mathrm{Bn}}$, $\mathrm{DBRF}_{\mathrm{At}}$, and $\mathrm{DBRF}_{\mathrm{Bt}}$ are the normal and tangential components of the DBRFs of drawbead A and drawbead B, respectively.

The strain by the bending of a combined drawbead C, $\varepsilon_{\mathrm{Cb}}$, is assumed to be expressed as the sum of those of basic drawbead A and basic drawbead B:

$$\varepsilon_{\mathrm{Cb}} = \varepsilon_{\mathrm{Ab}} + \varepsilon_{\mathrm{Bb}} \tag{36}$$

where $\varepsilon_{\mathrm{Ab}}$ and $\varepsilon_{\mathrm{Bb}}$ are the strains by the bending of basic drawbead A and basic drawbead B, respectively. When a sheet is drawn out through a combined drawbead C, the strain in the normal direction to the drawbead, $\varepsilon_{\mathrm{Cn}}$, and the strain in the tangential direction, $\varepsilon_{\mathrm{Ct}}$, are calculated by

$$\varepsilon_{\mathrm{Cn}} = \varepsilon_{\mathrm{Cb}} + \{(1+r)\sigma_{\mathrm{Cn}} - r\sigma_{\mathrm{Ct}}\}\left[\frac{\overline{\sigma}^{(1-n)/n}}{K^{1/n}(1+r)}\right] \tag{37}$$

$$\varepsilon_{\mathrm{Ct}} = \{-r\sigma_{\mathrm{Cn}} + (1+r)\sigma_{\mathrm{Ct}}\}\left[\frac{\overline{\sigma}^{(1-n)/n}}{K^{1/n}(1+r)}\right] \tag{38}$$

where σ_{Cn} and σ_{Ct} are respectively the stresses caused by the normal and tangential components of the combined DBRF.

Fig. 8 shows an example of partition of a combined drawbead. A circular-and-stepped drawbead is separated into a single circular drawbead and a stepped drawbead. Here, the assumption is made that the BHFs acting on both sides of the basic drawbeads, BHF_1 and BHF_2, can be represented as the blank holding force, BHF, divided by the length ratios, as shown below:

$$\mathrm{BHF}_1 = \mathrm{BHF}\frac{L_1}{L_0} \tag{39}$$

$$\mathrm{BHF}_2 = \mathrm{BHF}\frac{L_2}{L_0} \tag{40}$$

where L_0, L_1, and L_2 are the lengths of a combined drawbead, a circular drawbead, and a stepped drawbead, respectively. Furthermore, it is assumed that the thickness of the sheet entering the stepped drawbead is equal to that of the sheet drawing out the circular drawbead.

5. Verification

To verify the reliability of the expert drawbead model developed, the DBRF and bead-exit pre-strain predicted by the expert models of double circular drawbead and circular-and-stepped drawbead are compared with those obtained from the experiments.

5.1. Double circular drawbead

The sectional view of the double circular drawbead die set used in the experiment for verification is shown in Fig. 9. Four sets of double circular drawbeads with different drawbead heights ($h = 2$, 3, 4.5, and 6 mm) are manufactured. For different lubricating conditions, P-340N and BWD-610 are used. During the testing, the radius of the drawbead shoulder (R_s) and BHF are kept 3.8 mm and 156.8 N/mm, respectively.

The comparison of the DBRFs associated with two lubricants and four drawbead heights between prediction and measurement is shown in Fig. 10. Predictions by the expert model agree well with

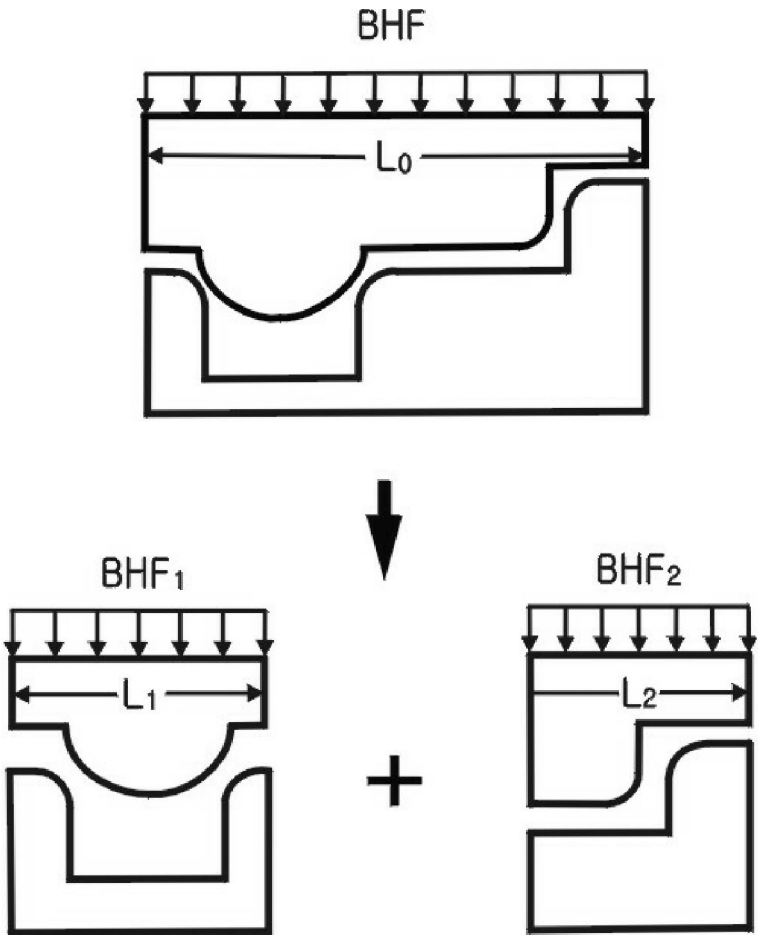

Fig. 8. Partition of a combined drawbead into basic drawbeads.

measurements. The DBRFs of the P-340N lubricated sheet are higher than those of the BWD-610 lubricated sheet. The relationship between drawbead height and DBRF is almost linear and proportional.

Fig. 11 shows the comparison of the pre-strains associated with two lubricants and four drawbead heights between prediction and measurement. It shows that bead-exit pre-strains do not increase linearly like DBRFs but increase gently. The deviation between prediction and measurement becomes larger as drawbead height increases. This indicates that the Bauschinger effect and rate-sensitivity should be considered in the calculation of bead-exit pre-strain, as pointed by Stoughton (1988).

5.2. Circular-and-stepped drawbead

Fig. 12 shows a sectional view of the circular-and-stepped drawbead die set employed in this verification. The dimension of the circular-and-stepped drawbead and the process variables are as follows:

Drawbead height (h): 3, 6 mm
Radius of stepped drawbead shoulder (R): 3, 4 mm

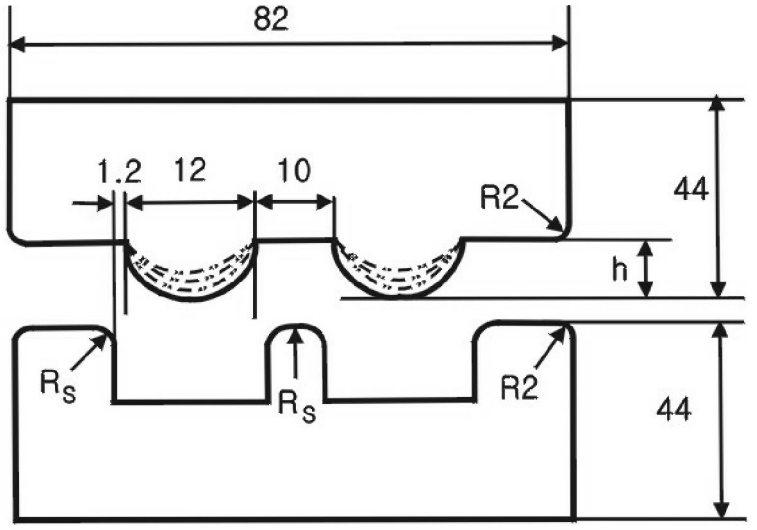

Fig. 9. Sectional view of a double circular drawbead die set.

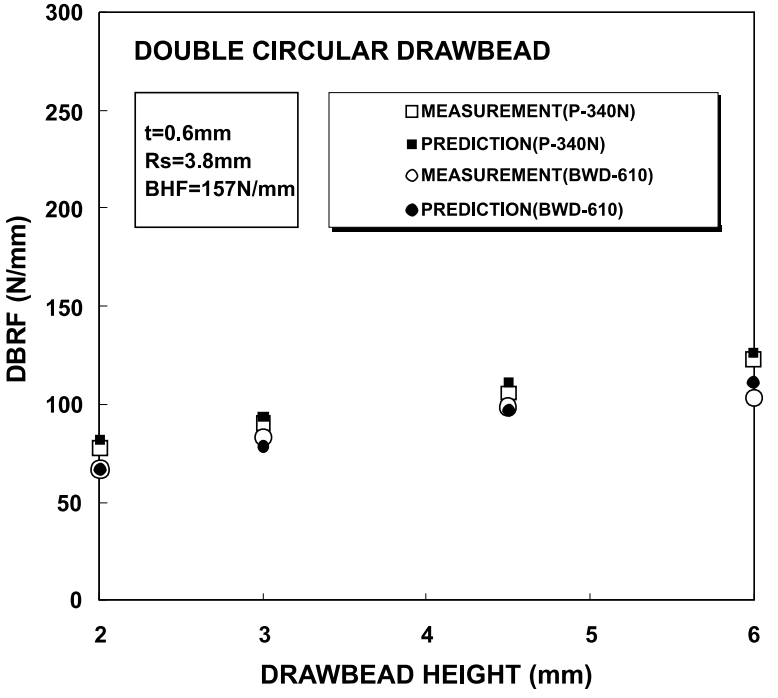

Fig. 10. Comparison of DBRFs for various lubricants and drawbead heights between prediction and measurement in a double circular drawbead.

BHF: 230, 344 N/mm
Lubricant: P-340N, BWD-610

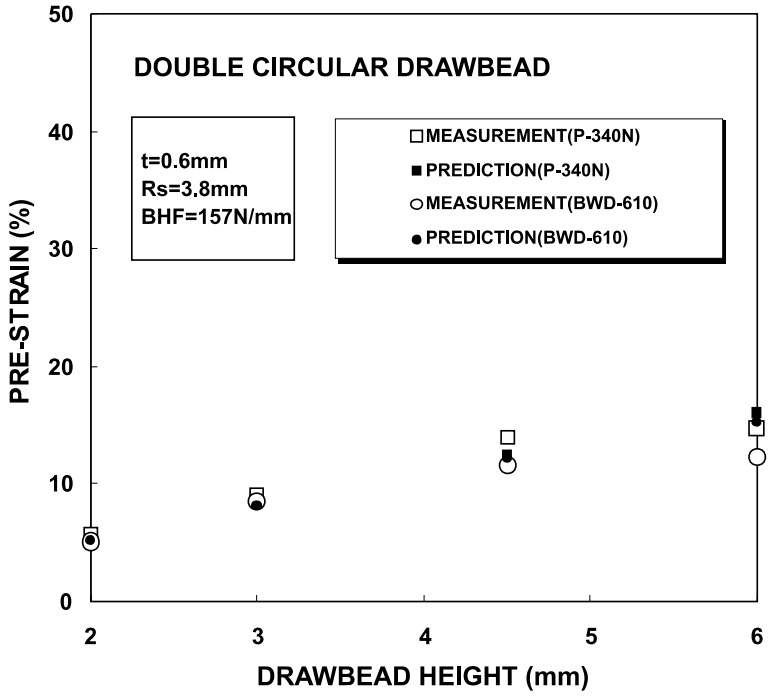

Fig. 11. Comparison of pre-strains for various lubricants and drawbead heights between prediction and measurement in a double circular drawbead.

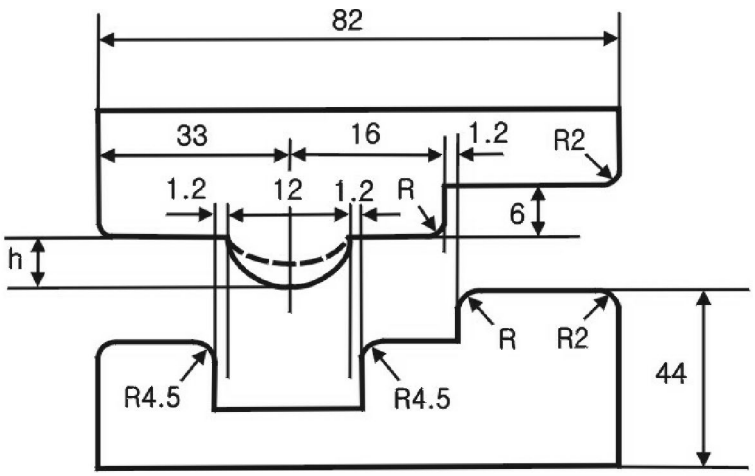

Fig. 12. Sectional view of a circular-and-stepped drawbead die set.

The comparison of the DBRF associated with the lubricant and radius of a stepped drawbead shoulder between prediction and measurement is shown in Fig. 13. The prediction by the expert model agrees well with the measurement, while the DBRFs of the P-340N lubricated sheet are a little higher than those of the

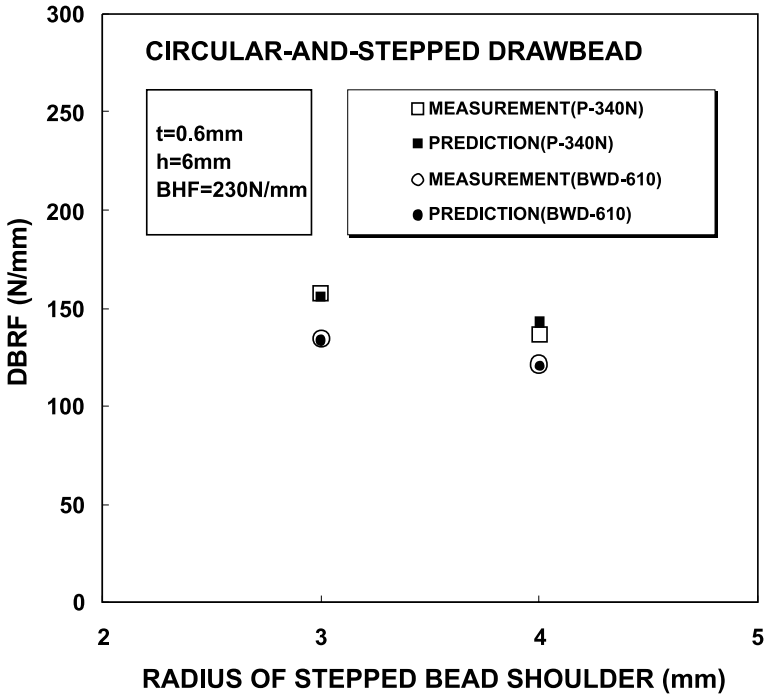

Fig. 13. Comparison of DBRFs for various lubricants and radii of stepped drawbead shoulder between prediction and measurement in a circular-and-stepped drawbead.

BWD-610 lubricated sheet. Due to the bending, the DBRFs decrease as the radius of stepped drawbead shoulder increases.

Fig. 14 shows the comparison of the pre-strains concerned with lubricants and radii of the stepped drawbead shoulder between prediction and measurement. Predictions agree quite well with measurements. The measured pre-strain decreases as the radius of a stepped drawbead shoulder increases as the DBRF does. Since the friction coefficient of the P-340N lubricated sheet is bigger than that of the BWD-610 lubricated sheet, the measured pre-strain of a P-340N lubricated sheet is higher than that of a BWD-610 lubricated sheet.

6. Conclusions

The expert drawbead model suitable for FEM analysis of sheet metal forming processes is developed, based on a mathematical model. The conclusions induced in the development of expert drawbead models are summarized as follows:

1. The expert model of the basic drawbead positioned with an arbitrary angle in the material moving direction is developed, which can predict DBRF and bead-exit pre-strain.
2. The expert model of the combined drawbead is developed by summing those of the basic drawbeads.
3. Since the difference in drawing characteristics of the drawbead between mathematical model and experimental measurement is mainly caused by the friction, the friction coefficient corrected by the multiple regression method is used in the expert model for a precise prediction.

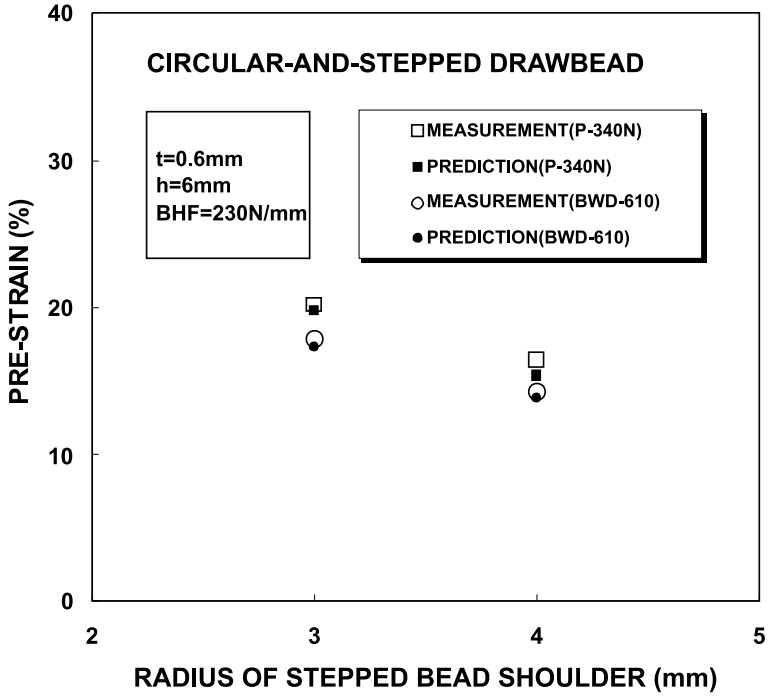

Fig. 14. Comparison of pre-strains for various lubricants and radii of stepped drawbead shoulder between prediction and measurement in a circular-and-stepped drawbead.

Acknowledgements

This work was supported in part by the Korea Science and Engineering Foundation (KOSEF) through the Engineering Research Center for Net Shape and Die Manufacturing at Pusan National University. The authors would like to thank Dr. S.S. Han and Mr. K.C. Park in POSCO for providing drawbead tester for the experiments.

References

Cao, J., Boyce, M.C., 1993. Drawbead penetration as a control element of material flow. SAE930517. Sheet-Metal and Stamping Symposium, Detroit.

Carleer, B.D., Meinders, T., Hu tink, H., 1996. Equivalent drawbead model in finite element simulations. Numerical Simulations of 3-D Sheet Metal forming Processes (NUMISHEET'96), Michigan, USA, pp. 25–31.

Demeri, M.Y., 1993. Drawbeads in sheet metal forming. J. Mater. Engng. Perf. 2 (6), 863–866.

Kim, Y.S., Kim, K.S., 1991. A study on friction-constraint of draw bead (I). Proc. Korean Soc. Mech. Engng. Korea, pp. 120–124.

Kojima, M., 1993. Effect of drawbead on press-load property in deep drawing of cylindrical shell. J. Jpn. Soc. Technol. Plast. 34, 1009–1018.

Levy, B.S., 1983. Development of a predictive model for draw bead restraining force utilizing work of Nine and Wang. J. Appl. Metal Working 3 (1), 38–44.

Meinders, M., Geijselaers, H.J.M., Hu tink, J., 1998. Implementation of plastic thickness strain in an equivalent drawbead model based on a penalty constraint method. Simulation of Material Processing: Theory, Methods and Applications (NUMIFORM'98). Enchede, Netherland. pp. 911–916.

Nine, H.D., 1978. Drawbead forces in sheet metal forming. Mechanics of Sheet Metal Forming. pp. 179–211.

Nine, H.D., 1982. New drawbead concepts for sheet metal forming. J. Appl. Metal Working 2 (3), 185–192.
Stoughton, T.B., 1988. Model of drawbead forces in sheet metal forming. Proceedings of the 15th IDDRG, Dearborn, USA and Toronto, Canada. pp. 205–215.
Sunaga, H., Yoneda, K., Makinouchi, A., 1996. Finite element modeling of drawbead in sheet metal forming. Numerical Simulations of 3-D Sheet Metal Forming Processes (NUMISHEET'96). Michigan, USA, pp. 186–190.
Ujohara, S., Frubayashi, T., Sakamoto, T., 1988. Simulation of forming severity on autobody panels using a CAD system – analysis of drawbead and its control. Proceedings of the 15th IDDRG. Dearborn, USA and Toronto, Canada, pp. 243–250.
Wang, N.M., 1982. A mathematical model of drawbead forces in sheet metal forming. J. Appl. Metal Working 2 (3), 193–199.
Wang, N.M., Shah, V.C., 1991. Drawbead design and performance. J. Mater. Shaping Tech. 9 (1), 21–26.
Weinmann, K.J., Sanchez, L.R., 1988. A general computer model for plane strain sheet flow and its application to flow between circular drawbeads. Proc. 15th IDDRG, Dearborn, USA and Toronto, Canada, pp. 217–226.
You, Y., Hong, P.Y., Yu, R.X., 1998. Calculation of drawbead restraining forces associated with kinematics hardening rule. Simulation of Material Processing: Theory, Methods and Applications (NUMIFORM'98), Enchede, Netherland, pp. 905–910.